LBL-17396
Preprint

Lawrence Berkeley Laboratory
UNIVERSITY OF CALIFORNIA

Materials & Molecular
Research Division

Submitted to Journal of Chemical Physics

REACTIVE SCATTERING OF $Na(3^2P_{3/2})$ + HCl

M.F. Vernon, H. Schmidt, P.S. Weiss,
M.H. Covinksy, and Y.T. Lee

July 1985

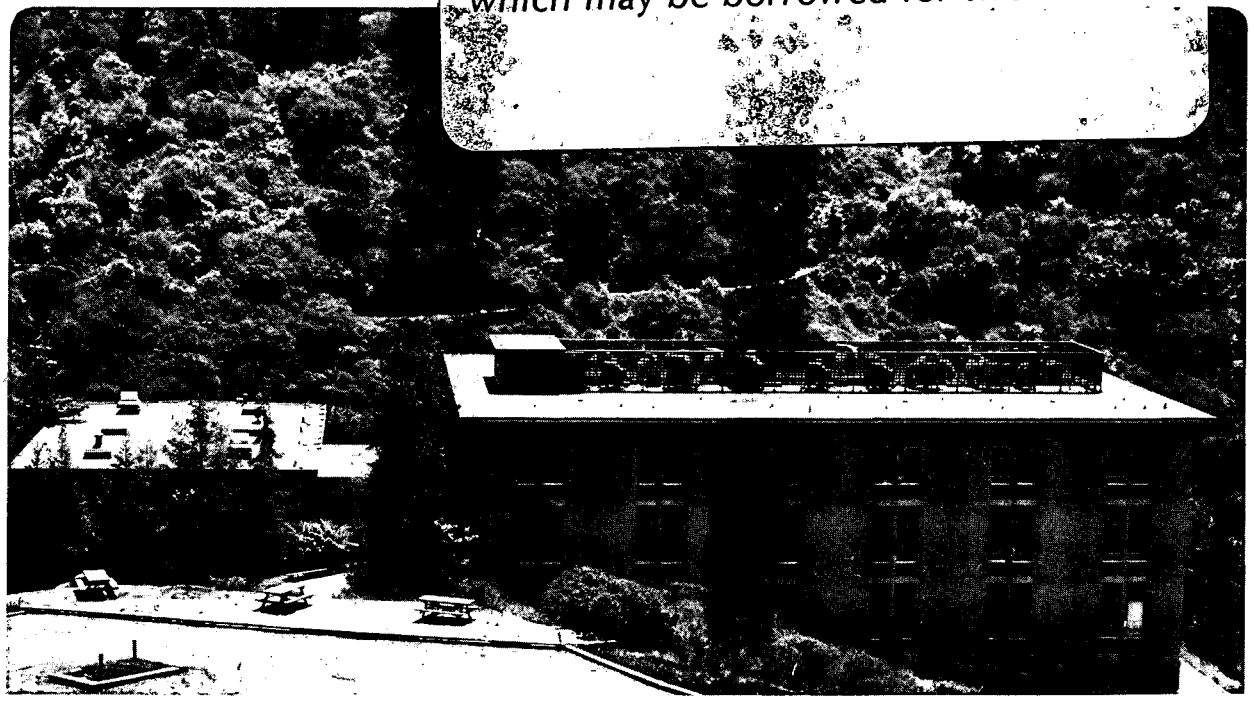

Prepared for the U.S. Department of Energy under Contract DE-AC03-76SF00098

DISCLAIMER

REACTIVE SCATTERING OF $Na(3^2P_{3/2})$ + HCl

M.F. Vernon[a], H. Schmidt[b], P.S. Weiss, M.H. Covinksy, and Y.T. Lee

Materials and Molecular Research Division
Lawrence Berkeley Laboratory and
Department of Chemistry, University of California
Berkeley, California 94720 USA

ABSTRACT

The reaction of electronically excited Na(3P) atoms with HCl has been studied in a crossed molecular beams experiment. Detailed measurements of the laboratory angular and velocity distributions of the reactively scattered NaCl product at 5.4 kcal/mole collision energy have allowed determination of the product center-of-mass translational and angular distributions. These experimental results are compared to the DIPR-DIP model of electron transfer reactions. The broad translational energy distribution is in qualitative agreement with the DIPR-DIP model, but the angular distribution exhibits reduced intensity for scattering perpendicular to the relative velocity vector which cannot be reproduced by the DIPR-DIP model. The preferred transition state configuration, Na-Cl-H, is consistent with what would be predicted by a diffuse 3P orbital where the Na atom appears ion-like and opposite to that given by the dominant term in the long range multipolar expansion of the neutral reactant potential.

---

a. Persent Address: Department of Chemistry, Columbia University, New York, New York, 10027.
b. Permanent Address: Freie Universitat Berlin, Fachbereich Physik (FB-20), Institut fur Molekulphysik, 1000 Berlin 33, West Germany.

INTRODUCTION

The study of reaction dynmamics by the crossed molecular beams method has historically been confined to collisions of ground state atoms and molecules. Notable exceptions are metastable states of the rare gas[1] or oxygen atoms.[2] The availability of stable, single frequency tunable dye lasers has recently allowed molecular beam studies involving short lived, electronically excited atoms. A series of papers by Hertel et al.[3-6] on the dynamics of collisional quenching of $Na^*(^2P_{3/2})$ and the works of Zare and coworkers[7-10] on chemiluminescence reactions of $Ca(^1P)$ atoms are pioneering examples.

The current experimental work was undertaken hoping to further our understanding of the dynamics of simple atom–diatomic molecule reactions where one of the reactants, $Na(3^2P_{3/2})$, is in an excited electronic state. HCl was chosen as a scattering partner because the reaction is 4.68 kcal/mol endothermic in the ground electronic state. This endothermicity allows one to study the interaction between translational and electronic energy in promoting NaCl formation.

The ground state reactions of the alkali–hydrogen halide family have been extensively studied by the molecular beam technique, including the efficiency of vibration, rotation and translation for promoting reaction.[11-13] Some ab initio[14] and semiempirical[15] potential energy surfaces are available and several classical trajectory studies[16] of reactions on these surfaces have been reported. Related theoretical studies of the H + HL mass combination where H and L stand for heavy and light atoms have been published.[17-19] Polanyi[20,21] has reported measurements

of the relative reaction cross sections for the Na + HCl (v,J) reaction for v = 1 - 4, J = 5 - 15. The vibrational enhancement indicated gas kinetic reaction cross sections. The dependence of the reaction cross section on the rotational quantum number was rationalized in terms of the preferred HCl - Na orientations for reaction.

In addition to the effect of electronic excitation on the reaction dynamics, the experiments described below can also measure the effect of the alignment and orientation of the $Na^*(3P_{3/2})$ charge distribution (created by optical pumping of sodium with linearly or circularly polarized laser radiation) on the reactive scattering. The alignment and orientation dependence and the reaction dynamics of higher excited states of Na will be the subject of a future investigation.

EXPERIMENTAL ARRANGEMENT

We have modified our universal, crossed molecular beams machine to allow laser excitation of Na in the collision region in the manner developed by Hertel. Figure 1 shows the experimental topology. Characteristics of the basic apparatus are given elsewhere.[13] Briefly, two supersonic beams are crossed, under single collision conditions, at right angles (beam overlap volume $\sim 10^{-2}$ cm^3) in a liquid nitrogen cooled, 1×10^{-7} torr vacuum chamber. Scattered product is detected with a mass spectrometer which can rotate in the plane defined by the two reactant beams. The mass spectrometer detector consists of an electron bombardment ionizer, quadrupole mass filter, and a Daly ion counter, enclosed in a triply differentially pumped, ultra-high vacuum chamber.

The experimental improvements described below include the development of a stable, seeded, Na atom source and the ability to excite a sizeable fraction of the Na atoms in the collision volume to the $3^2P_{3/2}$ excited state by the method of optical pumping.

A. Sodium Atom Beam Source

The sodium atom beam is produced by a rare gas seeded supersonic expansion from a two chamber stainless steel oven. The main oven section, the reservoir for the molten sodium metal, is heated by thermal coaxial heating cable (SEMCO, Inc.) brazed into contact with the oven body. At the top of the reservoir is a stainless steel gas inlet tube affixed onto a miniconflat flange and sealed by a .005 inch thick nickel gasket. The gas inlet tube is radiatively heated by a tungsten ribbon. Rare gases, introduced through the inlet tube, enable the average velocity of the sodium atoms to be varied over the range 1.0 - 3.0 x 10^5 cm/sec at a constant nozzle temperature, here chosen to be 740°C.

The nozzle chamber consists of a 3.0 inch long, .25 inch diameter stainless steel tube, heated by thermal coax heating cable brazed into contact with the stainless steel tube. The nozzle aperture is formed by drilling a .004-.006 inch diameter hole in a .020 inch thick stainless steel disk, which is welded onto the stainless steel tube. This additional chamber allows the nozzle to be substantially hotter than the reservoir, thus preventing the formation of sodium clusters during the expansion.

The oven chambers are surrounded by two levels of radiation shielding. The temperatures of the reservoir and nozzle are actively stabilized to

±2°C of any desired set point. This is necessary to maintain stable intensity and velocity for the sodium beam.

The central portion of the Na beam is skimmed by a single piece, heated, stainless steel skimmer. The diameter of the skimmer aperture is .045 inch diameter and is located .25 - .30 inches from the nozzle. The skimmer is also heated by coaxial heating cable.

The dimensions of the sodium beam at the collision region (1 mm tall by 3 mm wide) are determined by a rectangular aperture made from razor blades located in the second differential pumping region. The angular divergence of the Na beam is 1°. Heat radiated from the skimmer is sufficient to prevent clogging of the defining slit from Na condensation.

Ultra high purity rare gases, and an all metal, leak tight gas inlet system were found to be necessary to avoid slow clogging of the nozzle.

B. HCl Beam

The HCl beam was formed from a heated stainless steel tube with an interchangeable nozzle affixed on the end. A platinum electron beam aperture (Ted Pella, Inc.) of 70 micron diameter was used in this study. The nozzle temperature was actively stabilized to 180°C to prevent HCl cluster formation. Typically, 350 torr HCl nozzle backing pressure was used. A low pressure regulator, in addition to the standard cylinder regulator, was necessary to stabilize the delivery pressure at these low values. A rectangular aperture located in the second differential pumping region defines the transverse HCl beam profile to be 3mm tall and 3 mm wide at the collision region with an angular divergence of 3°. The HCl velocity distribution was derived from previously measured HCl velocity distributions

using the same apparatus but at a higher nozzle temperature (350°C). The average velocity of the high temperature distribution was multiplied by the ratio of the square root of the two nozzle temperatures to give the average velocity at the lower nozzle temperature. The value obtained, $8.45*10^4$ cm/sec, is consistent with 99 percent HCl rotational relaxation in the adiabatic expansion. Unrelaxed, the HCl average velocity would have been $7.23*10^4$ cm/sec. The full width at half maximum spread in the HCl velocities was assumed unchanged from the high temperature value of 20 percent.

C. Optical Preparation of $Na(3^2 P_{3/2})$

The creation of a large, stationary fraction of $Na(3^2P_{3/2})$ atoms, (whose natural lifetime is 16.6 nsec) by optical pumping has been exhaustively and elegantly studied by Hertel and coworkers.[22-26] Their experimental technique has been adopted here. Briefly, the selection rule for the change in total angular momentum, $\Delta F = \pm 1$ or 0, insures that all atoms excited from $^2S_{1/2}(F=2) \longrightarrow {}^2P_{3/2}(F=3)$ return to the $^2S_{1/2}$ $(F = 2)$ state by spontaneous emission. Thus, the sodium atom behaves as a simple two level system composed of the $^2S_{1/2}$ $(F = 2)$ and $^2P_{3/2}(F = 3)$ levels when the laser is tuned to this transition. Assuming statistical population of the ground state hyperfine levels before the atoms enter the laser beam, a maximum steady state excitation of 31.25 percent of the Na beam to the $^2P_{3/2}$ state can be achieved.

Several details are pertinent to realizing this maximal excitation efficiency. Power broadening must be less than 60 MHz, the separation of the $^2P_{3/2}(F=2)$ and $^2P_{3/2}$ $(F = 3)$ hyperfine (HF) levels. If this condition

is not met and the $^2P_{3/2}(F=2)$ level is excited, it can spontaneously decay to the $^2S_{1/2}(F=1)$ ground state HF level and would be lost from further optical pumping cycles. As the power broadening follows the spatial laser intensity profile, it is important to expand the laser beam so that the central portion is not power broadened beyond 60 MHz. Secondly, the sodium beam angular divergence along the laser beam propagation direction produces an associated transverse doppler shift. If this doppler shift is larger than 60 MHz, then some fraction of the sodium beam will be shifted off the $^2P_{3/2}(F=3)$ resonance. For Na seeded in He, this restricts the angular divergence to 1°, the angular spread of the Na beam in this study.

Even with these precautions there remains uncertainty in the fraction of atoms excited by laser optical pumping to the $3^2P_{3/2}$ (F=3) HF level. Relative fluorescence measurements as a function of the laser power density show a saturation effect, but tell nothing about the coupling to the $3^2P_{3/2}(F=2)$ HF level which can remove atoms from the desired two level system. The coupling arises from the small amount of laser energy resonant with the $3^2S_{1/2}(F=2) \longrightarrow 3^2P_{3/2}(F=2)$ transition (even when the laser frequency is locked to the $3^2S_{1/2}(F=2) \longrightarrow 3^2P_{3/2}(F=3)$ transition) which can optically pump atoms to the $3^2S_{1/2}(F=1)$ ground state. Empirically, in the scattering work of Schmidt and coworkers,[27] a 12 percent reduction in the inelastic $Na^+ + Na(3S) \longrightarrow Na^+ + Na(3P)$ transition was observed when the sodium beam was optically pumped. Unfortunately, in the present Na + HCl scattering experiments, there is no feature in the angular or velocity distributions which can be uniquely

assigned to ground state Na(3S) scattering. If such a feature can be found, its depletion by laser excitation of the Na atoms would measure the effective Na fraction optically pumped to the $3^2P_{3/2}$ state. Consequently, in the data analysis below, different values of the excitation efficiency, η, are analyzed. When the conclusions derived are dependent on the assumed value of η, they will be noted.

A combination of commercial camera lenses is used to image the sodium fluorescence onto a phototube (RCA IP28) as outlined by Fischer and Hertel.[3] In this way, any spatial dependence of the fluorescence intensity can be observed, as well as the average polarization characteristics of the fluorescence from only the collision volume.

The signal from the camera phototube, after current amplification (Keithly Model 427) drives a lock-in stabilizer (Lansing 80-214) which corrects for frequency drifts. The necessary reduction of the transverse doppler width noted above causes a 50 percent pumping loss if the laser frequency drifts 20 MHz off line center. The lock-in stabilizer produces a DC correction voltage and an AC (510 Hz) modulation reference frequency. These are appropriately scaled and summed, then input to the external voltage controlled frequency drive of the Coherent Radiation Model 599-21 dye laser scan electronics. The laser stability is sufficient for greater than 24 hours of continuous operation.

D. Angular Distribution Measurement Procedure

Most of the data acquisition is computer controlled. Five basic quantities are measured at each laboratory angle in an angular scan. These are (1) the Na fluorescence intensity (LF), (2) the mass spectrometer

signals with the laser on and HCl beam on (L_+X_+), (3) the laser off and HCl beam on (L_-X_+), (4) the laser on and HCl beam off (L_+X_-), and (5) the laser off and HCl beam off (L_-X_-). With the laser off, the difference

$$[\,(L_-X_+) - (L_-X_-)] \propto \frac{d\sigma}{d\Omega}\,(3^2S_{1/2}) \qquad (3)$$

is proportional to the 3S ground state scattering. When the laser is on the mass spectrometer signal will have contributions of a fraction η from $3^2P_{3/2}$ scattering and a fraction $(1-\eta)$ from $3^2S_{1/2}$ scattering. The following combination of the four mass spectrometer signals is proportional to the $3^2P_{3/2}$ differential cross section

$$\frac{d\sigma}{d\Omega}\,(3^2P_{3/2}) \;\alpha\; (L_+X_+ - L_+X_-) - (1-\eta)^*\,(L_-X_+ - L_-X_-) \qquad (4)$$

To obtain the four mass spectrometer data channels, the HCl beam is 100 percent amplitude modulated by the 150 Hz tuning fork chopper mounted on a water cooled copper block in the HCl beam differential chamber, and the laser beam is 100 percent amplitude modulated at 3 Hz by a stepping motor controlled beam stop.

For all data presented, the error bars for the mean are one standard deviation for the statistical error associated with the finite signal count, or the variance of the mean of the actual measurements, whichever is larger. Typically, four separate angular scans are averaged to obtain approximately 10 percent error (1σ) in the derived 3P distributions. The total counting time at each angle is usually eight minutes.

E. Doppler Shift Measurements of Na Velocity Distributions

The sodium velocity distribution is measured by monitoring the doppler shifted fluorescence from the 45° laser crossing, and scanning the laser frequency. The fluorescence intensity has the characteristic patterns shown in Fig. 2. There are four peaks. The two narrow and intense peaks are from the orthogonal Na beam intersection used in the optical pumping. Their separation is the ground state HF splitting (1.77 GHz) minus a weighted sum of the $3^2P_{3/2}$ HF structure determined by the fluorescence transition strengths from the $3^2P_{3/2}$(F=3, 2 and 1) HF levels. Empirically, this weighting produces a splitting of 1.67-1.70 GHz for the narrow peaks. This separation is consistent with the splitting derived from the fringe spacing (1.5 GHz) of the Fabrey-Perot etalon and with the measured direction of the center-of-mass velocity vector for the Na + HCl scattering. If only the 1.77 GHz ground state HF splitting is used, the calculated center-of-mass velocity vector shifts 2° towards the Na beam from where it is empirically observed.

The two broad, red shifted peaks of Fig. 2 are the doppler shifted analogs of the orthogonal crossing peaks. The separation, in GHz, between the orthogonal and associated 45° crossing transition, $\Delta\nu$, is related to the average flow velocity, v_o, in cm/sec, by the equation

$$v_o(\text{cm/sec}) = \frac{c\Delta_\nu}{\nu_o \sin(45^\circ)} = 8.33*10^4*\Delta\nu(\text{GHz})$$

where c is the speed of light and ν_0 is the transition frequency. The Na beam velocity distribution is found by fitting the observed doppler fluorescence profile to the functional form

$$n(v)dv = Cve^{-\beta(v-v_0)^2} dv \qquad (7)$$

appropriate for a number density velocity distribution. The distribution has been weighted by 1/v as the faster moving atoms spend less time in the laser beam and execute fewer spontaneous radiation cycles. The full width at half maximum velocity spread is typically 20 percent.

F. Product Velocity Measurements

Time-of-flight measurements of the product velocity distributions at selected detector angles are obtained by the cross correlation method. The scattered products are correlated to the modulation of the laser by a 255 channel pseudo-random sequence encoded onto a spinning disk placed in the path of the laser beam. By cross correlating the modulated fluorescence, the empirical laser modulation function is directly obtained which incorporates the averaging caused by the variation in slit size and rotation synchronization of the spinning disk.

Modulation of the laser affects equal densities of the 3S and 3P sodium atoms because for every Na atom excited to the 3P state, one is removed from the ground state. The 3P atoms contribute a positive mass spectrometer signal whereas the 3S atoms contribute a negative mass spectrometer signal under laser modulation.

The different reactivities of the two electronic states determine the TOF pattern observed. The contributions from the excited state at each laboratory angle, compared to those from ground state, are derived from the angular data by the equation

$$R(\theta) = \frac{d\sigma^*/d\Omega(\theta)}{d\sigma/d\Omega(\theta)} = \frac{(L_+X_+ - L_+X_-) - (1-\eta)(L_-X_+ - L_-X_-)}{\eta(L_-X_+ - L_-X_-)} \qquad (8)$$

EXPERIMENTAL RESULTS

An independent check of the accuracy of the reactant beam velocities is provided by the sodium ground electronic state reactive NaCl angular distribution measured at the 5.38 kc/m collision energy. At this collision energy, only 0.7 kc/m is available for product translation. The maximum NaCl center-of-mass recoil velocity is only 4×10^3 cm/sec which is less than 3 percent of the relative velocity between Na and HCl. Consequently, the observed laboratory angular distribution of NaCl shown in Fig. 3 reflects only the distribution of center-of-mass angles from the velocity dispersion of the reactant beams. The maximum of the NaCl angular distribution located at 40° in the laboratory frame is correctly predicted by these beam velocities. A product flux distribution which is independent of the details of the recoil angular and energy distributions, but consistent with the maximal recoil velocity, reproduces the observed angular variation as shown in Fig. 4.

The Newton diagrams corresponding to the two collision energies for which data will be presented are shown in Fig. 5. The full widths at half-maximum for the reactant beam velocities, as well as the distribution of center-of-mass angles generated using the average flow velocity of one beam and the half-maximum velocities of the other beam, are shown as hatched areas on the Newton diagrams. The approximate angular broadening caused by these distributions, $\Delta\theta_{cm}$, is also given.

The maximum center-of-mass product velocity allowed in the Na(3P) reaction, U^{*}_{NaCl}, is determined from the reaction endothermicity of 4.68 kcal/mol, the photon energy of 48.43 kcal/mol, and the translational energy corresponding to the average velocity of each beam. The maximum laboratory scattering angles where product can appear from the excited state reaction are also indicated.

The angular distributions measured at masses 23 (Na^{+}) and 58 ($NaCl^{+}$) without laser excitation at two collision energies are shown in Fig. 3. As noted above, the reaction Na(3S) + HCl-->NaCl + H at 5.38 kcal/mol collision energy is slightly above the reaction threshold . For the mass combination of this reaction, and the small amount of energy available for product translational motion, the product angular distribution contains no detailed information on the product energy or center-of-mass scattering angle distribution with the current detector resolution and velocity dispersion of the reactant beams.

The mass 23 angular distribution measured at the 5.38 kcal/mole collision energy is predominately elastic or inelastic scattering. A minor reactive contribution is detected at mass 23 near $\Theta = 40^{\circ}$ from

fragmentation of NaCl in the electron bombardment ionization process. As the detection sensitivities for mass 23 and mass 58 ions in the experiment are approximately equal, the fragmentation ratio, $Na^+/NaCl^+$, for NaCl product formed near threshold and ionized by 160 volt electrons can be estimated by subtracting different multiples of the mass 58 purely reactive angular distribution from the mass 23 predominately nonreactive angular distribution. The family of curves generated using multiplicative factors in the range 1-2 is shown in Fig. 6. Assuming negligible depletion of the large angle, non-reactive scattering for this near threshold collision energy, a fragmentation ratio of 50-55 percent produces a smooth, monotonic mass 23 angular distribution for the corrected, non-reactive sodium scattering. Variation of the energy of the ionizing electrons in the interval 50-200 volts does not markedly change the fragmentation ratio.

A similar analysis of the non-reactive Na(3S) scattering at the 19.4 kcal/mol collision energy is shown in Fig. 6. At this collision energy, the mass 23 data is dominated by NaCl reaction product ion fragments and correction for the fragmentation is difficult. Unlike the 5.38 kcal/mol mass 23 angular distribution, there is no obvious pure, nonreactive scattering at laboratory angles beyond 15° to enable an interpolation through the angular range dominated by reaction product ion fragmentation. The nonreactive scattering expected to contribute to laboratory angles less than 15° is masked by the effusive Na background from the beam source. The best estimate from the 19.4 kcal/mole data gives a fragmentation ratio of near 70 percent. Fragmentation ratios less than 70 percent always leave a residual bump near the center-of-mass in the mass 23 angular distribution.

The mass 23 and 58 angular distributions derived from Eq. (4), assuming different Na*(3P) excitation efficiencies for both collision energies are shown in Fig. 7. A 50 percent error in the fraction of Na atoms assumed to be in the 3P state significantly affects the derived Na(3P) differential cross sections for the 19.4 kcal/mole collision energy data, while the 5.38 kcal/mole collision energy data are unchanged within the stated measurement errors.

Laser correlated time-of-flight (TOF) measurements were performed at selected angles for masses 23 and 58 at the 5.38 kcal/mole collision energy. Time-of-flight measurements of the ground electronic state scattering have not been performed. To obtain the TOF for the reaction of Na*(3P) from the laser correlated TOFs, the latter were corrected according to Eq. (8) using computed ground state TOF distributions. As stated above, at this near threshold collision energy, the ground state reactive scattering is severely convoluted by the distribution of center-of-mass angles. The TOF distributions obtained from the center-of-mass distribution derived from the mass 58 ground state angular distribution are expected to closely approximate the true ground state TOFs. The corrected, mass 23 distributions derived differ little from the original laser correlated TOFs. The main effect is to boost the signal at 35°, 40°, and 45° for the channels near the center-of-mass. As the 3P state is approximately ten times more reactive, the corrected channels are displaced within their original statistical error. The corrected mass 23 TOF data are shown in Fig. 8. The TOF data at the laboratory angles 25° and 30° clearly exhibit a fast, Na(3P) elastic peak as well as a slower, broader, reactive ion fragment peak.

In general, the error in the assumed fraction of Na(3P) atoms in the collision volume can have a dramatic effect on the extraction of the TOF distribution for Na*(3P) scattering from the laser correlated TOF data. The relative weighting of the Na(3S) TOF to the laser correlated TOF depends on the ratio of the contribution of Na(3P) to Na(3S) atoms at that laboratory angle. In turn, this depends on what fraction of the Na atoms we assume to be Na*(3P). At the collision energy 5.38 kcal/mole, the laser induced signal is large compared to the ground state scattering signal. Large errors in the fraction of Na atoms excited does not significantly affect the derived center-of-mass energy and angle distributions. For the 19.4 kcal/mol collision energy, the ground state signal is comparable to the laser induced signal and the assumed value for the Na(3P) fraction can qualitatively affect the shape of the angular and TOF data used to obtain the center-of-mass product flux distributions.

The laser induced mass spectrometer signal was also studied as a function of the laser fluorescence intensity. The data obtained by attenuating the laser power over two orders of magnitude using neutral density filters shows a linear dependence within the experimental accuracy.

DATA ANALYSIS

The angular and velocity distributions measured at masses 23 and 58 in the scattering of Na(3P) + HCl can be reasonably ascribed to one of the following collision processes:

Reaction	$Na(3P) + HCl\ (v=0) \longrightarrow NaCl + H(^2S)$	(14)
	$Na(3P) + HCl\ (v=0) \longrightarrow NaH + Cl(^2P_{3/2})$	(15)
Quenching	$Na(3P) + HCl\ (v=0) \longrightarrow Na(3S) + HCl(v',J')$	(16)
Elastic or Rotational Inelastic		
	$Na(3P) + HCl\ (v=0) \longrightarrow Na(3P) + HCl(J')$	(17)

Analogous to the Na(3S) reactive scattering, NaCl product is expected to be favored over NaH. However, unlike the ground state scattering, the part of the mass 23 angular distributions which are from NaCl product do not have the same shape as the mass 58 distributions. If we followed the logic applied above to the Na(3S) scattering, we might conclude that there is significant Na(3P) scattering which can not be attributed to elastic or NaCl reactive scattering. As will be shown below, the differences are mainly due to the internal energy dependence of the NaCl fragmentation ratio in the electron bombardment ionization process.

From the ground state Na(3S) reactive scattering analysis, it was noted that at threshold and 15 kcal/mole above threshold, the NaCl fragmentation ratio changed from 50 to 70 percent. For the Na(3P) angular distributions, this ratio is not observed. The $NaCl^+$ signal is only 1/10 of the mass 23 signal even at the peak of angular distribution. Since the

highly internally excited NaCl produced by Na(3P) fragments by electron bombardment ionization, the mass 23 angular distribution is a more accurate measure of the true NaCl reactive product distribution. For example, a change in the fragmentation ratio from 90 to 92 percent for $NaCl^+$ will affect the mass 23 distribution by 2 percent while changing the mass 58 distribution by 20 percent. Since there is a rapid increase in the fragmentation ratio in the ground state reaction with increasing collision energy, and the $NaCl^+$ parent mass is a minor fragment ion in the excited state reaction, the mass 23 distribution is taken to reflect the true NaCl product distribution for the excited state reaction. Of course, allowance for Na(3P) elastic scattering must be done at small angles.

In the above discussion, it was assumed that all of the mass 23 data (corrected for elastic scattering) was from NaCl ion fragmentation, and that the contributions from NaH formation or quenching were unnecessary to account for any of the observed mass 23 intensity. Although NaH formation is not expected to compete with the NaCl formation, kinematics favors detection of NaCl product.

Center-of-mass NaCl product flux distributions were dervived from the experimental data using a computer program. The computer program accounts for the kinematic averaging caused by the distribution of reactant beam velocities and the finite spatial and temporal resolution of the detector. The program generates time-of-flight and angular distributions corresponding to an input center-of-mass distribution, which are then directly compared to the laboratory measurements. By trial and error, a center-of-mass distribution which best represents the measurements is found.

In the analysis of the 5.38 kcal/mole data the total reaction cross section was considered independent of the collision energy. The range of collision energies is sufficiently narrow in the experiment so this assumption should not introduce significant error, except near threshold where the reaction cross section might have a strong translational energy dependence.

For finding the best fit center-of-mass distributions, a numerical table specifying the probability of scattering at selected center-of-mass recoil velocities was found useful. The scattering angles and recoil speeds representing the table entries were distributed over the range of the observed product with a sampling density guided by the kinematic averaging induced by the spread of reactant velocities.

The best center-of-mass flux distribution is shown in Fig. 9 and compared to the experimental data in Fig. 8. Essentially exact agreement with the experimental data can be obtained if unrestricted variation of a sufficiently dense grid of the table entries is allowed. The resulting distribution is symptomatic of high parameter correlation and not uniquely determined by the data. The best fit distribution is a subjective compromise between faithful reproduction of the experimental data and meaningful parameter extraction. The energy averaged center-of-mass recoil angle distribution and the recoil angle averaged, center-of-mass energy distribution are given in Fig. 10 for the best fit distribution.

DISCUSSION

The Na* + HCl reaction has many of the expected features of a prototypical electron transfer "harpoon" reaction. The essence of this model is that during an early phase of the reaction, an ionic complex is formed by transfer of the Na^3P electron to HCl. If the electron transfer occurs rapidly compared to the nuclear motion, HCl^- should be formed with a distribution of internuclear separations given by a vertical projection of the HCl vibrational wavefunction onto a dissociative, repulsive region of the HCl^- potential. Due to the light mass of the H atom, if H does not interact strongly with Na^+, it should quickly separate from the Na^+/Cl^- ion pair which subsequently associates into a NaCl molecule under the influence of attractive coulombic forces.

A solveable, classical model for this type of reaction is the DIPR-DIP (Direct Interaction with Product Distributed as in Photodissociation) model orginated by Polanyi[28] and elaborated by Herschbach and coworkers.[29] Rettner and Zare[30] have recently extended and applied this model to chemiluminescent reactions.

The DIPR model is expected to be accurate for $A+BC \longrightarrow AB+C$ reactions which proceed first by release of the BC^- repulsive energy subsequently followed by A^+B^- attraction. Secondly, A^+ should interact weakly with the B^- and C atom while BC^- dissociates, and similary for C with A^+ and B^- while the latter pair associates. Clearly, a steep BC^- potential with large exothermicity will favor a short timescale for the release of the repulsive energy. In the Na + HCl reaction, the mass combination favors a rapid departure of the H atom. Using theoretical

potential curves for HCl and HCl^-,[31] the Frank Condon region accessible from the ground vibrational state of HCl predicts product translational energies in the range 10–40 kcal/mol. This compares favorably with the range observed in the experiment.

From the above discussion, it would appear that the Na* + HCl reaction would be an ideal candidate for the DIPR–DIP model. However, the DIPR model is based on the electron transfer occuring at relatively large reagent separation where the repulsive energy release occurs prior to product bond formation. The intermolecular distance where the electron transfer takes place is, to first order, calculated from the -23 kcal/mol vertical electron affinity of HCl(v=0)[31] and the +76 kcal/mol ionization potential of $Na(^3P)$. These values predict that the electron will transfer to HCl when the Na*–HCl separation is ~3.5 Å. However, the outer peak of the electron probability distribution for $Na(^3P)$ extends from 3–4 Å, with a maximum at 3.5 Å. This means that the electron jump occurs when the HCl molecule is already <u>within</u> the 3P orbital of Na*. The close proximity of the Na^+ ion may invalidate applying the DIPR model in this case. Instead of two distinct reaction phases characterized by sequential two-body interactions, the reaction might be more accurately viewed as a process in which the initial electron transfer is followed by repulsive energy release between the H atom and the Na^+Cl^- molecule as a whole.

The total reaction cross section is expected to be affected in approximately the same way by either Na electronic energy or HCl vibrational energy. This is because the vibrational excitation increases the HCl electron affinity while the electronic excitation reduces the Na

ionization potential. To first order, the reaction cross section will depend only on the energy difference between the Na ionization potential and the HCl electron affinity. Consequently, the enhancement of the reaction cross section for $Na(^3P)$ or vibrationally excited HCl,[20,21] is consistent with the "harpoon" model.

The center-of-mass product distribution is a good test of the applicability of the DIPR-DIP model. To apply the model we need to specify the distribution of product translational velocities. Within the DIP approximation, this would be given by projecting the HCl(v=0) nuclear wavefunction onto the HCl^- potential. For simplicity, since we do not know the distribution of HCl bond lengths when the electron jumps, we extract an optimal translational energy distribution from the experimental data by the kinematic relations of the DIPR model.

The center-of-mass angular distribution in the DIPR model allows for relative weighting of different HCl orientations at the moment of the electron jump. This weighting accounts for the anisotropic forces which might be present at the electron jump distance favoring certain reactant configurations or from a variation in the reaction probability with orientation. We assume that there is no correlation between product translational energy and the HCl orientational distribution and determine a best fit orientational distribution by optimizing the single parameter functional form given by Marron,[32]

$$T(\theta) = (1 + \cos\theta)^n$$

to the experimental data. Here θ is the diatomic orientation at the moment of the electron jump, and it depends on the product scattering angle and translational energy through the DIPR model assumptions as derived by Marron. See reference 32 for details.

From the best fit DIPR model to the experimental data, if the model is an accurate representation of the reaction mechanism, we learn about the distribution of the HCl bond lengths, the HCl bond orientation relative to the Na* atom, and the nature of the HCl^- potential in the Frank-Condon region. In Figs. 11 and 12 we show the best fits obtained using the DIPR model. Comparision of the DIPR model fit with the best fit coupled center-of-mass distributions shows the largest difference for scattering perpendicular to the relative velocity vector. In the DIPR model, it is not possible to have a small intensity along this scattering angle. However, the anisotropy parameter, n, is small (n~0.24) indicating that there is nearly an isotropic distribution for the HCl at the moment of the electron jump. The extracted reaction anisotropy favors the Na-Cl-H configuration. This is in accord with the predicted configuration if the valence electron is diffuse, i.e., Na^+ + Cl-H and not that of the dominant long range multipole interaction (quadrupole-dipole) which would favor Na-H-Cl. The translational energy distribution for the DIPR model fit is broad, with almost equal probability from 10-50 kcal/mol. This is within the predicted range of the DIPR-DIP model using the isolated HCl^- potential curve discussed previously.

Finally, if the DIPR model is qualitatively correct for the reaction of $Na(3P_{3/2})$ + HCl, higher energy Na electronic states should have nearly

the same product translational energy, as this is primarily determined by the $H-Cl^-$ repulsion after electron transfer. The additional electronic energy should appear as vibrational excitation of NaCl. The higher excited electronic states have a larger electron jump distance, and since the H atom will depart rapidly, the conversion of the potential energy of the Na^+-Cl^- ion pair at the electron jump distance to product translational energy will be small. On the other hand, if the repulsive energy release cannot be adequately described solely by the $H-Cl^-$ repulsion and the extent of NaCl bond formation or electronic symmetry has to be considered, then the translational energy distributions of products will depend on the electron jump distance and the level of electronic excitation. This question will be investigated in the future.

CONCLUSIONS

The results of a crossed molecular beam study of the $Na(3^2P_{3/2})$ + HCl reaction have been compared with a sequential two-body model (the DIPR model) which is known to sucessfully explain reactions characterized by long range electron transfer. Qualitatively, the experimental scattering is similar to what the DIPR model would predict using only theoretical data available from the literature. The differences between the observed scattering distributions and those which can be generated by optimizing the parameters of the DIPR model were concluded to originate from a breakdown in the assumption of sequential release of repulsive and attractive energy. This is consistent with the small internuclear distance of the

electron transfer, which imparts a degree of "concertedness" to the reaction. Future experiments on the reactions of higher electronic states of sodium will provide an interesting comparison on the validity of a two body sequential model.

ACKNOWLEDGMENT

This work was supported by the Director, Office of Energy Research, Office of Basic Energy Sciences, Chemical Sciences Division of the U.S. Department of Energy under Contract No. DE-AC03-76SF00098. H.S. wishes to thank the Deutsche Forschungsgemeinschaft for financial support.

REFERENCES

1. Robin Hennessy, Yoko Ono, and J. P. Simons, Mol. Phys., 43, 181 (1981).
2. R. Buss, P. Casavecchia, T. Hirooka, S. Sibener, Y. T. Lee, Chem. Phys. Lett., 82, 386 (1981).
3. A. Fischer, I. Hertel, Z. Phys. A., 304, 103 (1982).
4. I. Hertel and W. Stoll, J. App. Phys., 47, 214 (1976).
5. I. Hertel and W. Stoll, Adv. Atomic Mol. Phys., 13, 113 (1978).
6. H. Hermann and I. Hertel, Comments At. Mol. Phys., 12, 61, 85 (1982).
7. M. Prisant, C. Rettner, and R. Zare, Chem. Phys. Lett., 88, 271 (1982).
8. M. Prisant, C. Rettner, and R. Zare, J. Chem. Phys., 75, 2222 (1981).
9. C. Rettner and R. Zare, J. Chem. Phys., 75, 3636 (1981).
10. C. Rettner and R. Zare, J. Chem. Phys., 77, 2416 (1982).
11. F. Heismann and H. Loesch, Chem. Phys., 64, 43 (1982).
12. M. Hoffmeister, L. Potthast, and H. J. Loesch, Chem. Phys., 78, 369 (1983).
13. C. Becker, P. Casavecchia, P. Tiedemann, J. Valentini, Y. T. Lee, J. Chem. Phys., 73, 2833 (1980).
14. M. Chen, H. S. Schaefer, J. Chem. Phys., 72, 4376 (1980).
15. M. Shapiro and Y. Zeiri, J. Chem. Phys., 70, 5264 (1979).

16. I. Noorbatcha, N. Sathyamurthy, Chem. Phys., 77, 67 (1983) and references therein.

17. N. Hijazi and J. Polanyi, Chem. Phys., 11, 1 (1975).

18. K. Schulten, R. G. Gordon, J. Chem. Phys., 64, 2918 (1976).

19. H. Baer, Mol. Phys., 26, 369 (1973).

20. F. Bartoszek, B. Blackwell, J. Polanyi, and J. Sloan, J. Chem. Phys., 74, 3400 (1981) and references therein.

21. B. Blackwell, J. C. Polanyi, and J. C. Sloan, Chem. Phys., 30, 299 (1978).

22. N. Reiland, C. Schulz, H.-V. Tittes, and I. Hertel, Chem. Phys. Lett., 91, 329 (1982).

23. W. Reiland, G. Jamieson, H.-V. Tittes, and I. Hertel, Z. Phys. A., 307, 51 (1982).

24. W. Reiland, H. Tittes, I. Hertel, V. Bonacic-Koufecky, and Maurizio Persico, J. Chem. Phys., 77, 1908 (1982).

25. P. Botschwina, W. Meyer, I. Hertel, and W. Reiland, J. Chem. Phys., 75, 5438 (1981).

26. W. Reiland, H. Tittes, and I. Hertel, Phys. Rev. Lett., 48, 1389 (1982).

27. H. Schmidt, A. Bahring, E. Meyer, and B. Miller, Phys. Rev. Lett., 48, 1008 (1982).

28. P. J. Kuntz, M. H. Mok, J. C. Polanyi, J. Chem. Phys. 50, 4623 (1969).

29. D. P. Herschbach, Discussions of the Faraday Society, 55, 233 (1973).

30. M. G. Prisant, C. T. Rettner, R. N. Zare, J. Chem. Phys. 81, 2699 (1984).

31. J. N. Bardsley, J. M. Wadehra, J. Chem. Phys. 78, 7227 (1983).

32. M. Marron, J. Chem. Phys. 58, 153 (1973).

FIGURE CAPTIONS

Fig. 1 Schematic diagram of the experimental appartus showing the orientations of the two molecular beams, mass spectrometer detector and the laser used for optical pumping.

Fig. 2. Doppler shifted fluorescence for He (top) and Ne (bottom) seeded Na atom beams. Δf measures the $F=2 \longrightarrow F'=3$ transition shift. The bottom trace is a relative frequency standard derived from an etalon.

Fig. 3. Na(3S)/Na(3P) + HCl scattering angular distributions measured at the two collision energies at mass 23 (top) and mass 58 (bottom). The signal is measured in units of the experimentally observed count rates.

Fig. 4. Calculated and observed NaCl product angular distribution for the Na(3S) + HCl reaction. A constant product translational energy and recoil angle distribution was assumed.

Fig. 5. Newton diagrams for the Na(3P) + HCl system at the two collision energies measured in the experiment. The hatched areas show the FWHM velocity distributions at each beam, and the distribution of center-of-mass angles resulting from the reactant beam velocity spreads. The maximal NaCl product velocity is restricted to the circle drawn about the center-of-mass by conservation of energy. The laboratory angles tangent to these circles are the nominal maximum scattering angles for observation of NaCl product.

Fig. 6. Mass 23 angular distributions corrected for electron bombardment induced ion fragmentation of the NaCl reaction product assuming different fragmentation ratios.

Fig. 7. The derived Na(3P) + HCl scattering angular distributions at the two collision energies at mass 23 (top) and mass 58 (bottom) assuming an excitation efficiency of 25 percent. Error bars are 1 standard deviation of the mean. The signal is in units of the observed count rates. The dotted lines show the derived signal using excitation efficiencies of 30 percent and 5 percent.

Fig. 8. Experimental laser correlated time-of-flight distributions at mass 23 for the indicated laboratory angles. At 25° and 30°, elastic scattering of Na(3P) atoms can be easily seen. The slow, broader peak at all angles is assigned to NaCl product which fragments in the electron impact ionizer to Na^+. The solid line is the fit to the data given by the numerically determined center-of-mass scattering distribution.

Fig. 9. Optimal center-of-mass NaCl product flux distribution determined from the analysis of the TOF and angular data for the 5.38 kcal/mole collision energy.

Fig. 10. Translational energy averaged recoil angle distribution and recoil angle averaged translational energy distribution for the best fit center-of-mass scattering distribution.

Fig. 11. Best DIPR model fit to the experimental TOF data.

Fig. 12. Best DIPR model fit center-of-mass product flux distribution.

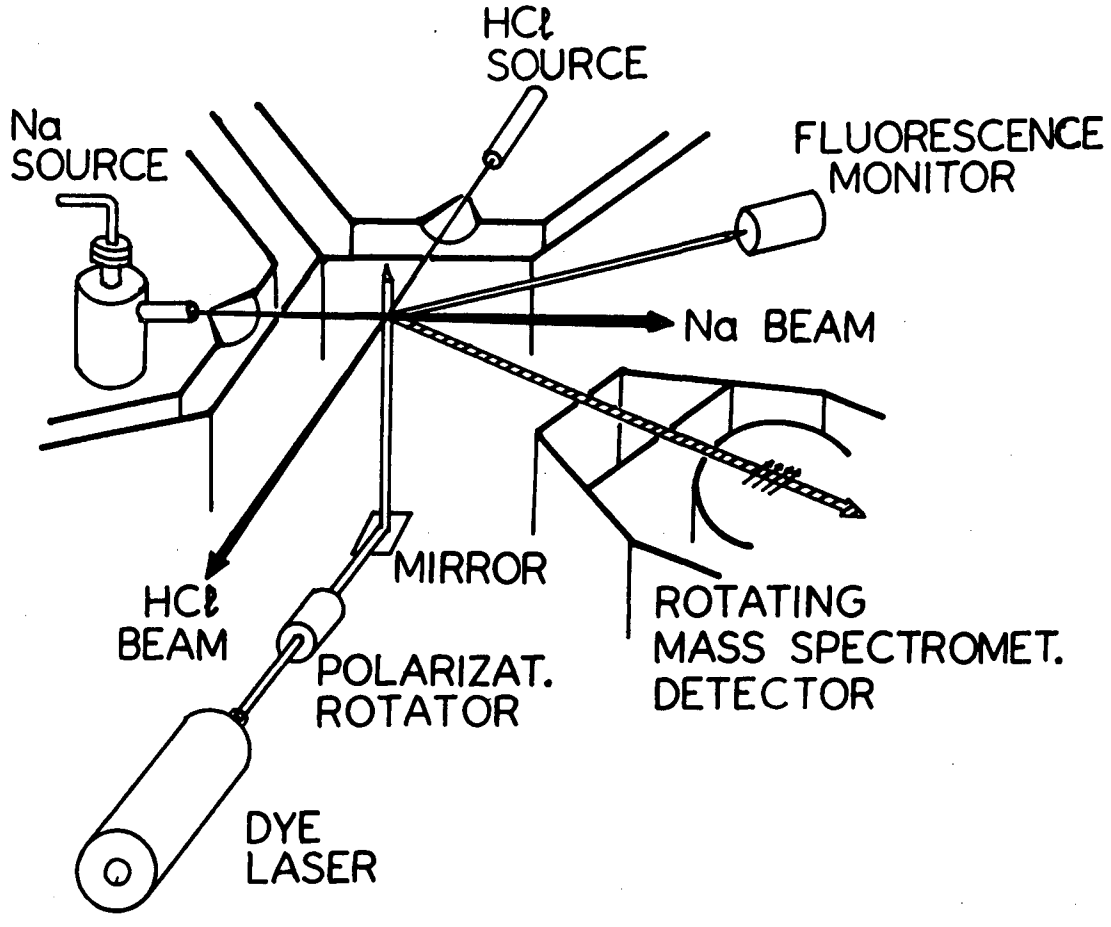

XBL 856-2877

Fig. 1

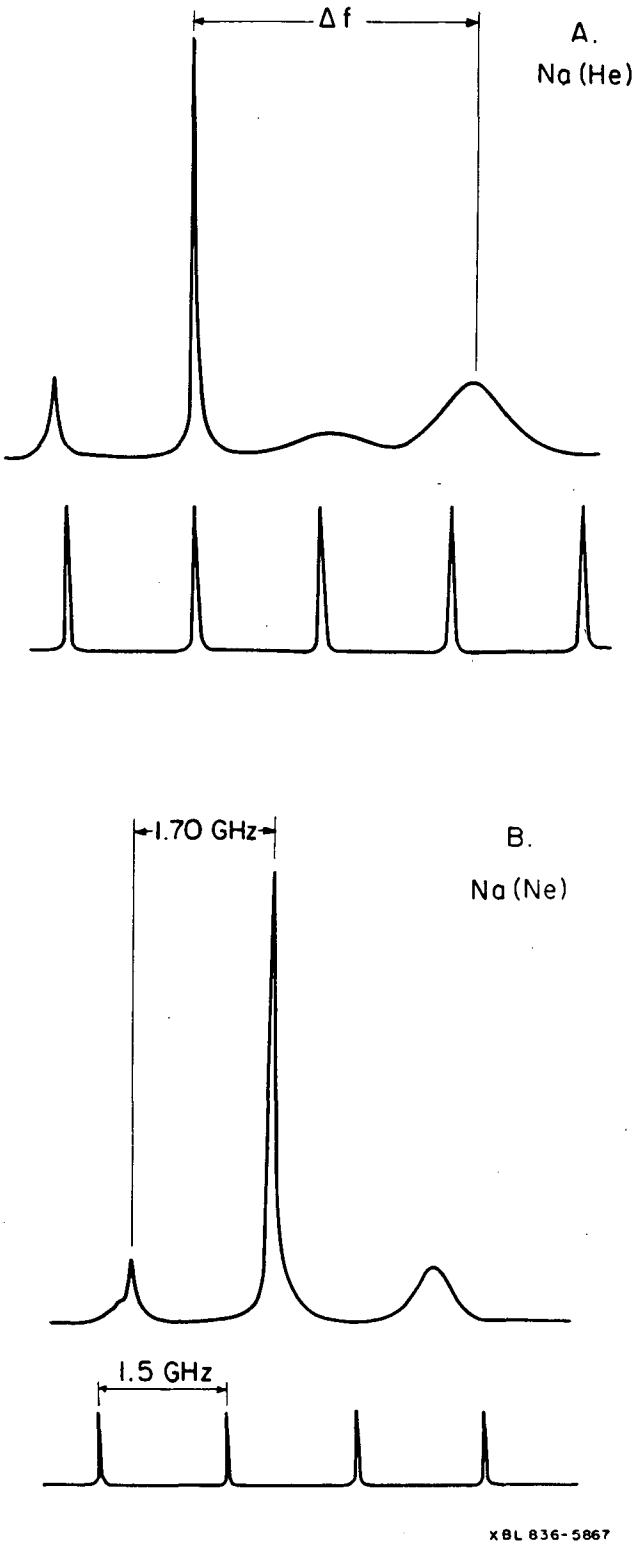

Fig. 2

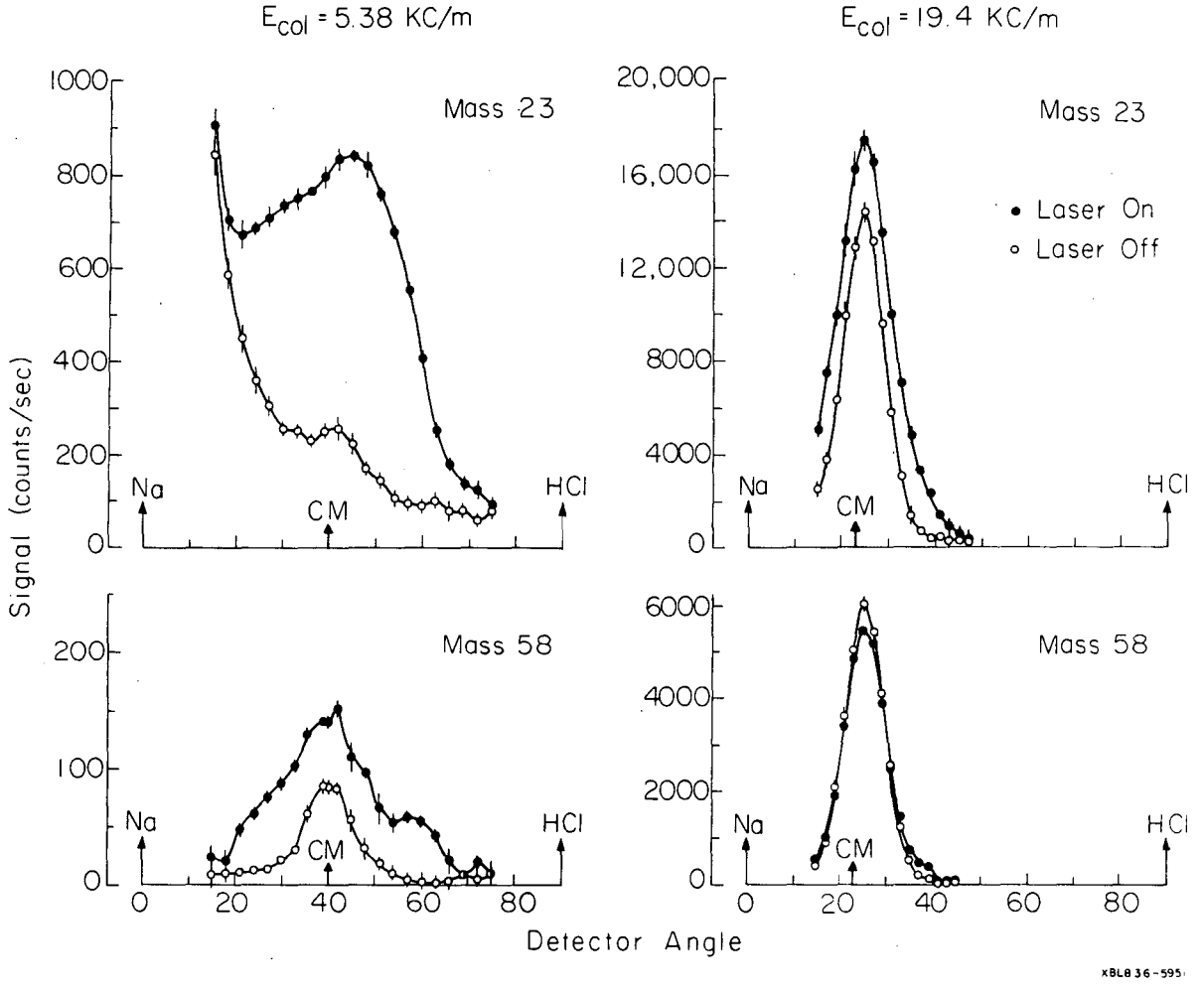
E_{col} = 5.38 KC/m
E_{col} = 19.4 KC/m
Mass 23
Mass 58
Laser On
Laser Off
Signal (counts/sec)
Detector Angle
Na
CM
HCl
1000
800
600
400
200
0
20,000
16,000
12,000
8000
4000
6000
2000
100
0
20
40
60
80
XBL836-595

Fig. 3

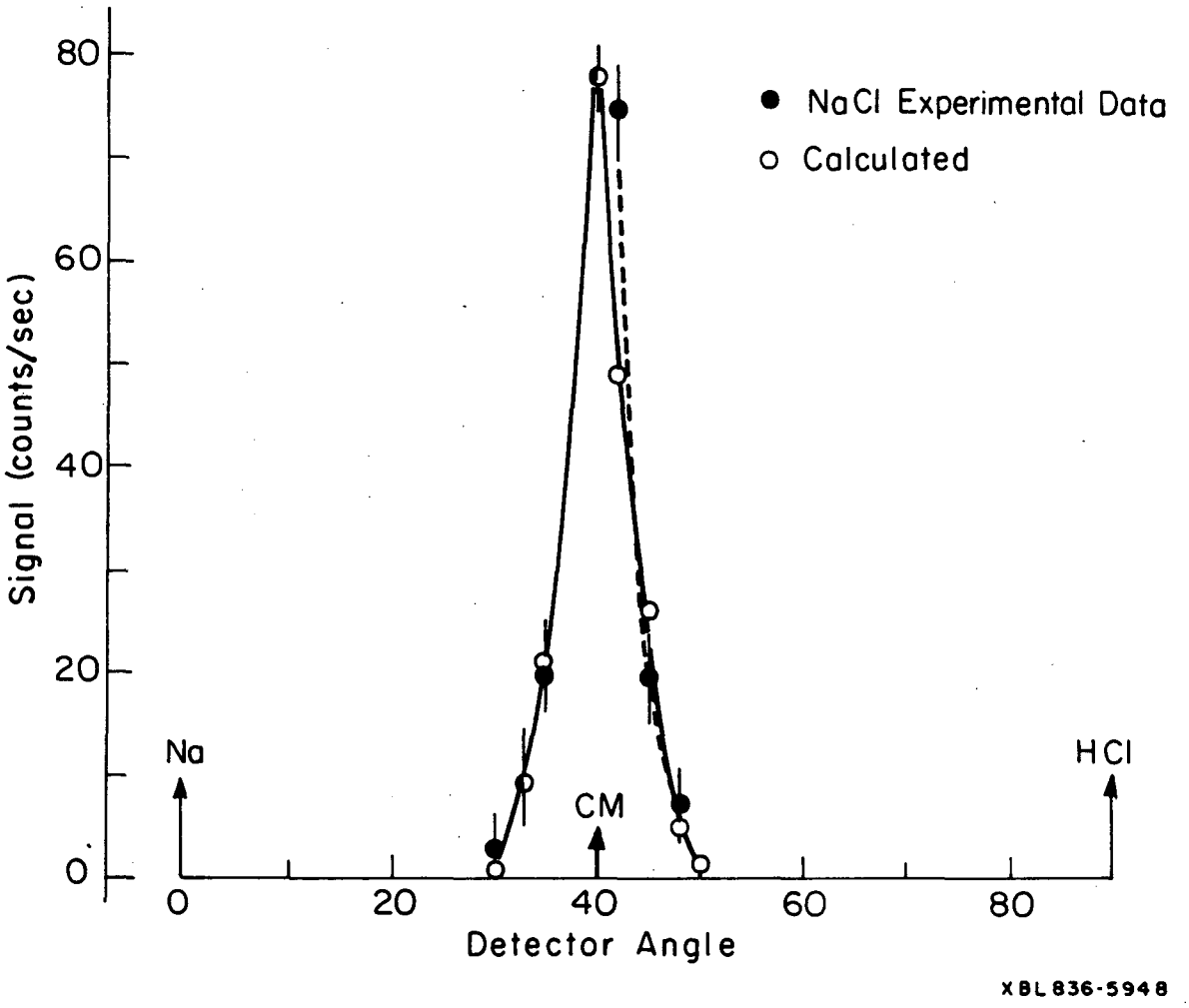
80
60
40
20
0
Signal (counts/sec)
NaCl Experimental Data
Calculated
Na
CM
HCl
0
20
40
60
80
Detector Angle
XBL836-5948

Fig. 4

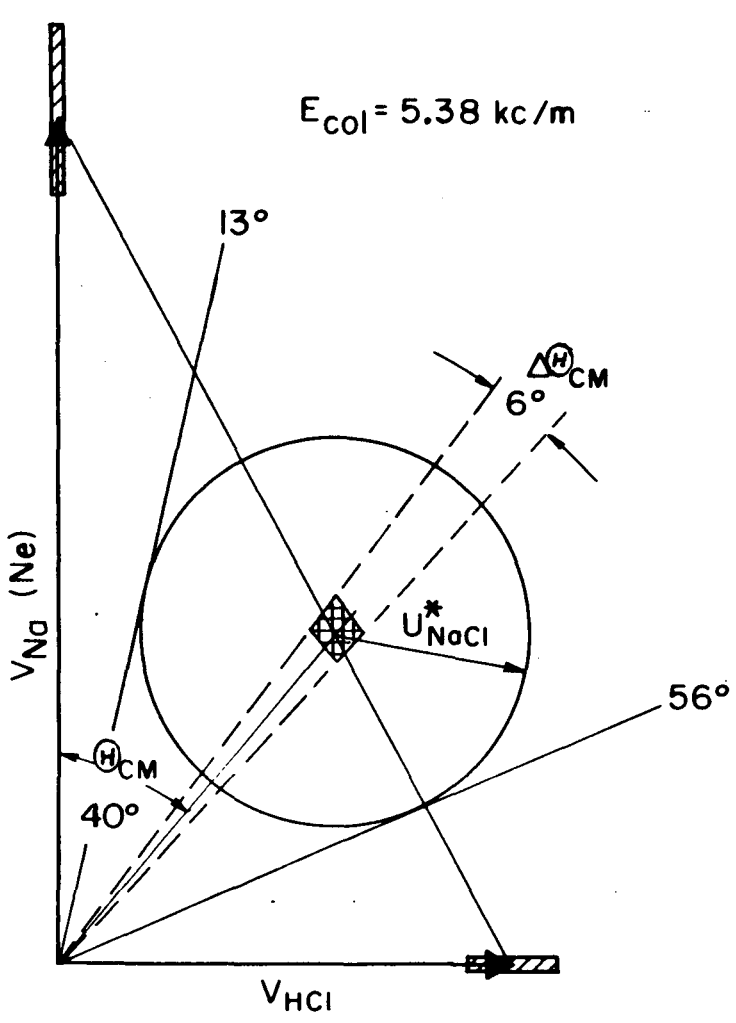

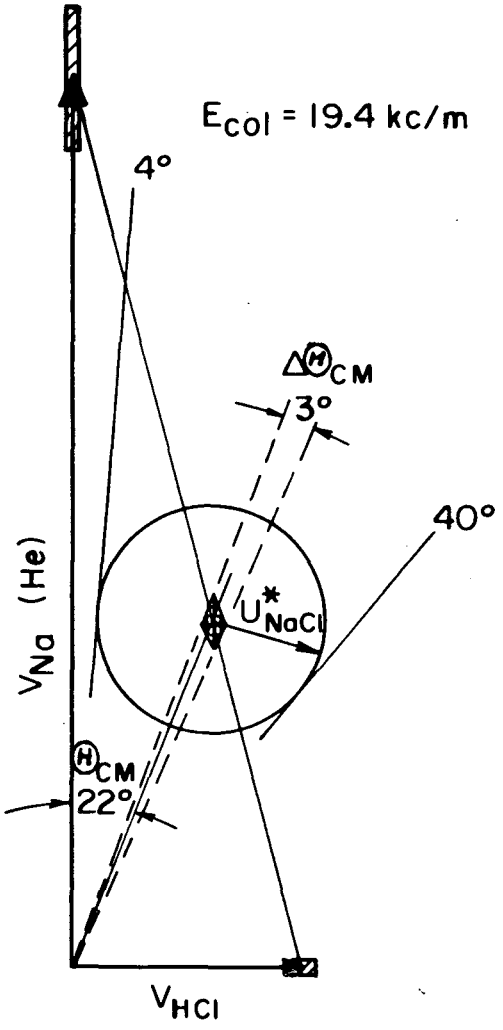

XBL 856-2878

Fig. 5

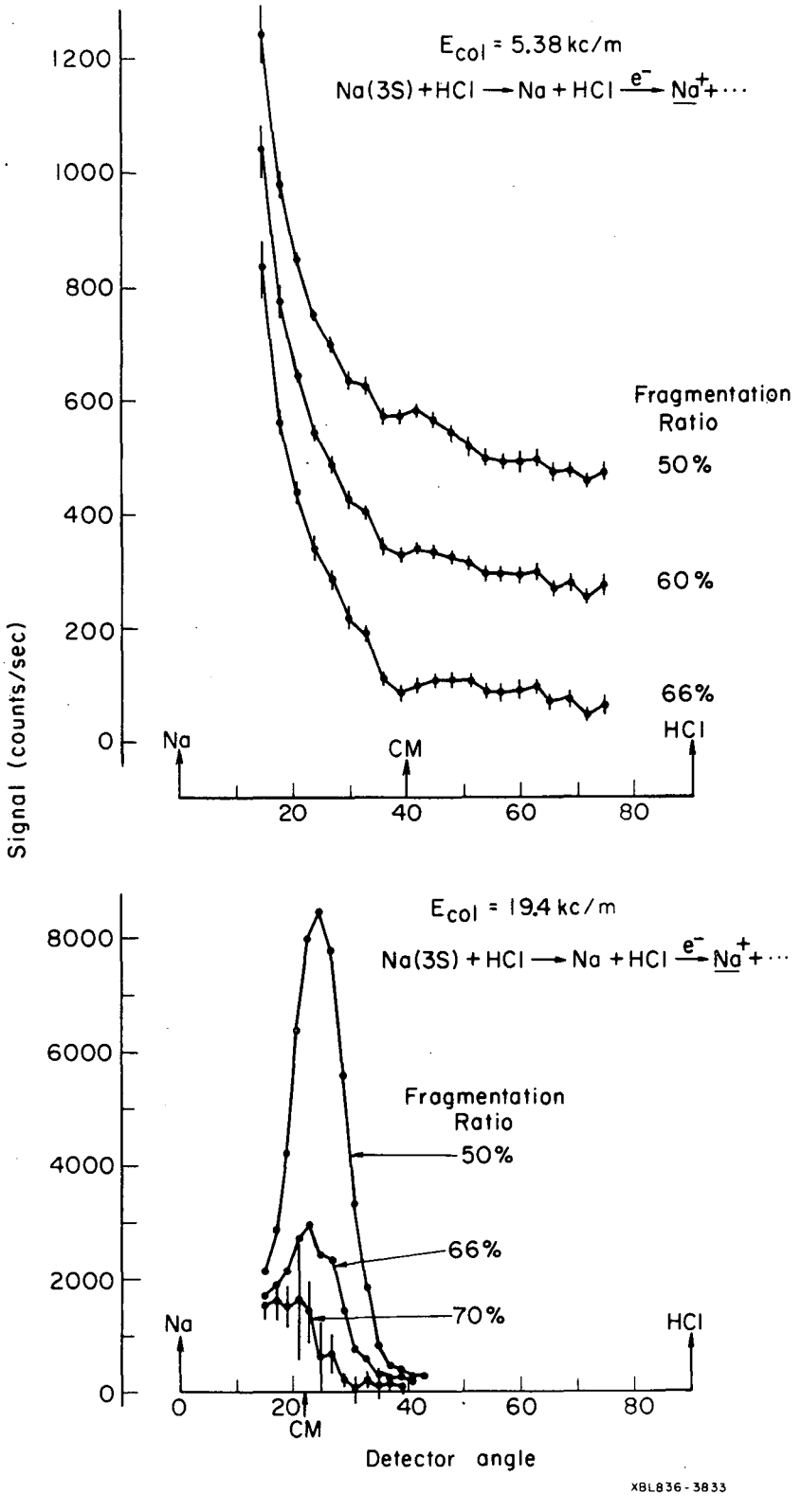
E_{col} = 5.38 kc/m
Na(3S) + HCl → Na + HCl $\xrightarrow{e^-}$ $\underline{Na}^+$ + ···
Fragmentation Ratio
50%
60%
66%
Signal (counts/sec)
1200
1000
800
600
400
200
0
Na
CM
HCl
20
40
60
80
E_{col} = 19.4 kc/m
Na(3S) + HCl → Na + HCl $\xrightarrow{e^-}$ $\underline{Na}^+$ + ···
Fragmentation Ratio
50%
66%
70%
8000
6000
4000
2000
0
Na
HCl
0
20
CM
40
60
80
Detector angle
XBL836-3833

Fig. 6

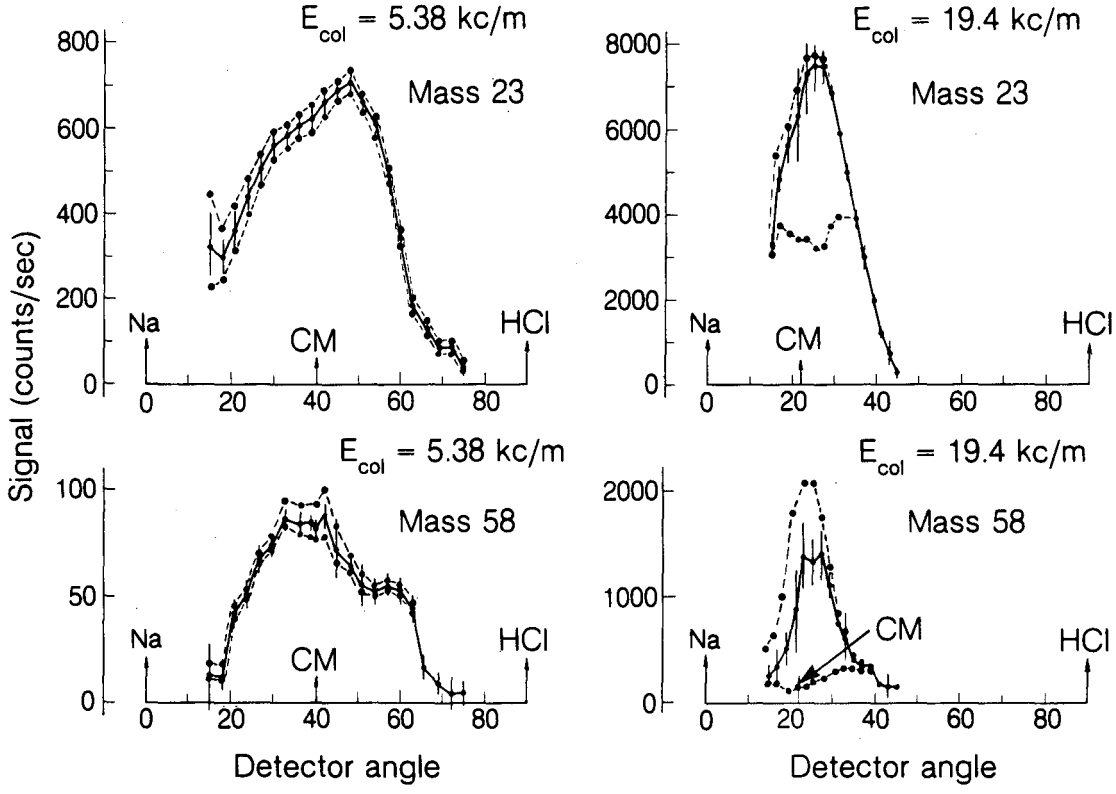
E_{col} = 5.38 kc/m
Mass 23
E_{col} = 19.4 kc/m
Mass 23
E_{col} = 5.38 kc/m
Mass 58
E_{col} = 19.4 kc/m
Mass 58
Signal (counts/sec)
Na
CM
HCl
Detector angle
XBL 836-3835

Fig. 7

$$Na\ (3P) + HCl \rightarrow NaCl + H \xrightarrow{e^-} \underline{Na}^+ + \ldots$$

$$E_{col} = 5.38\ kc/m$$

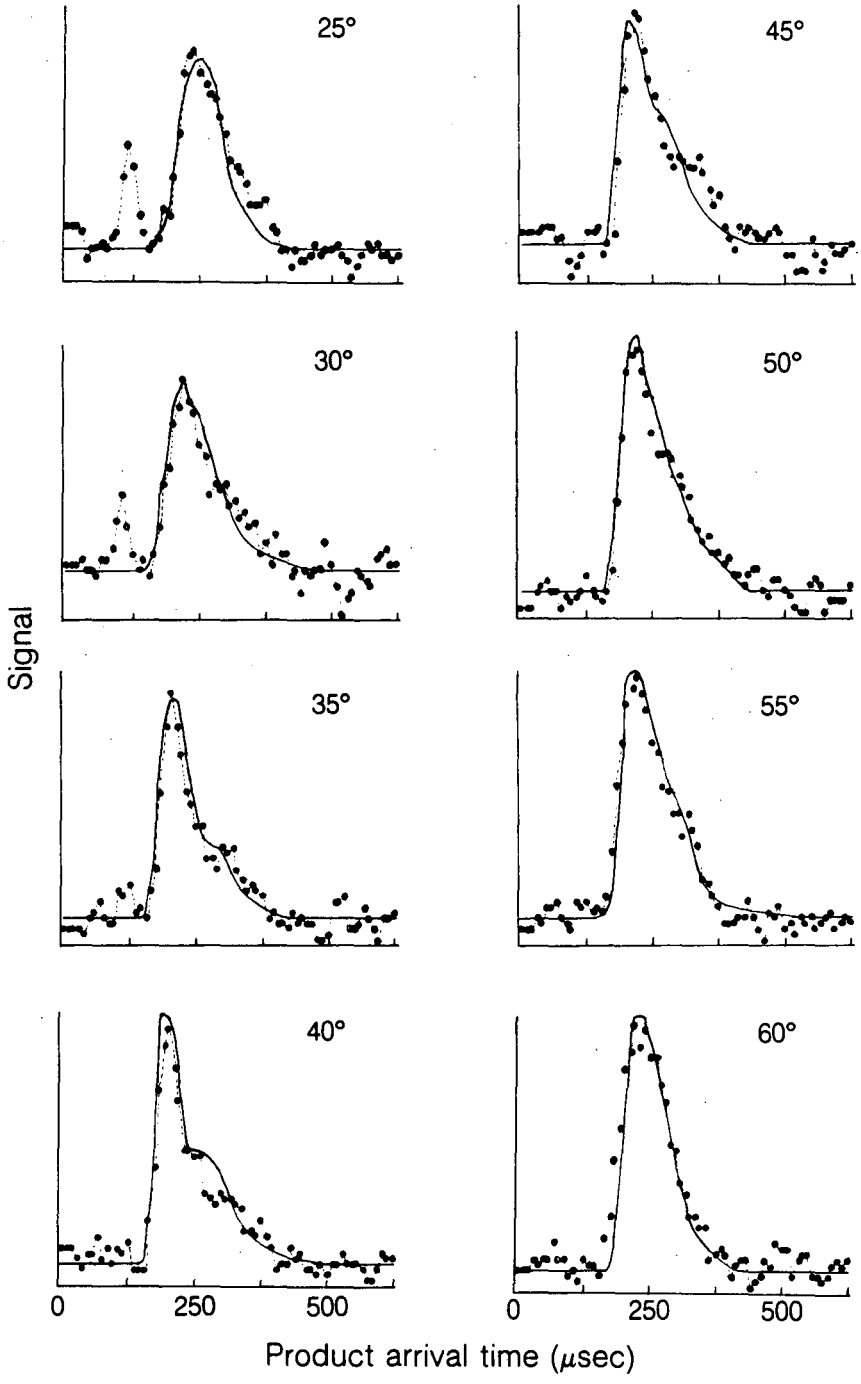

XBL 837-10708

Fig. 8

$$Na(3P) + HCl \longrightarrow NaCl + H \xrightarrow{e^-} \underline{Na}^+ + \cdots$$
$$E_{col} = 5.38\ kc/m$$

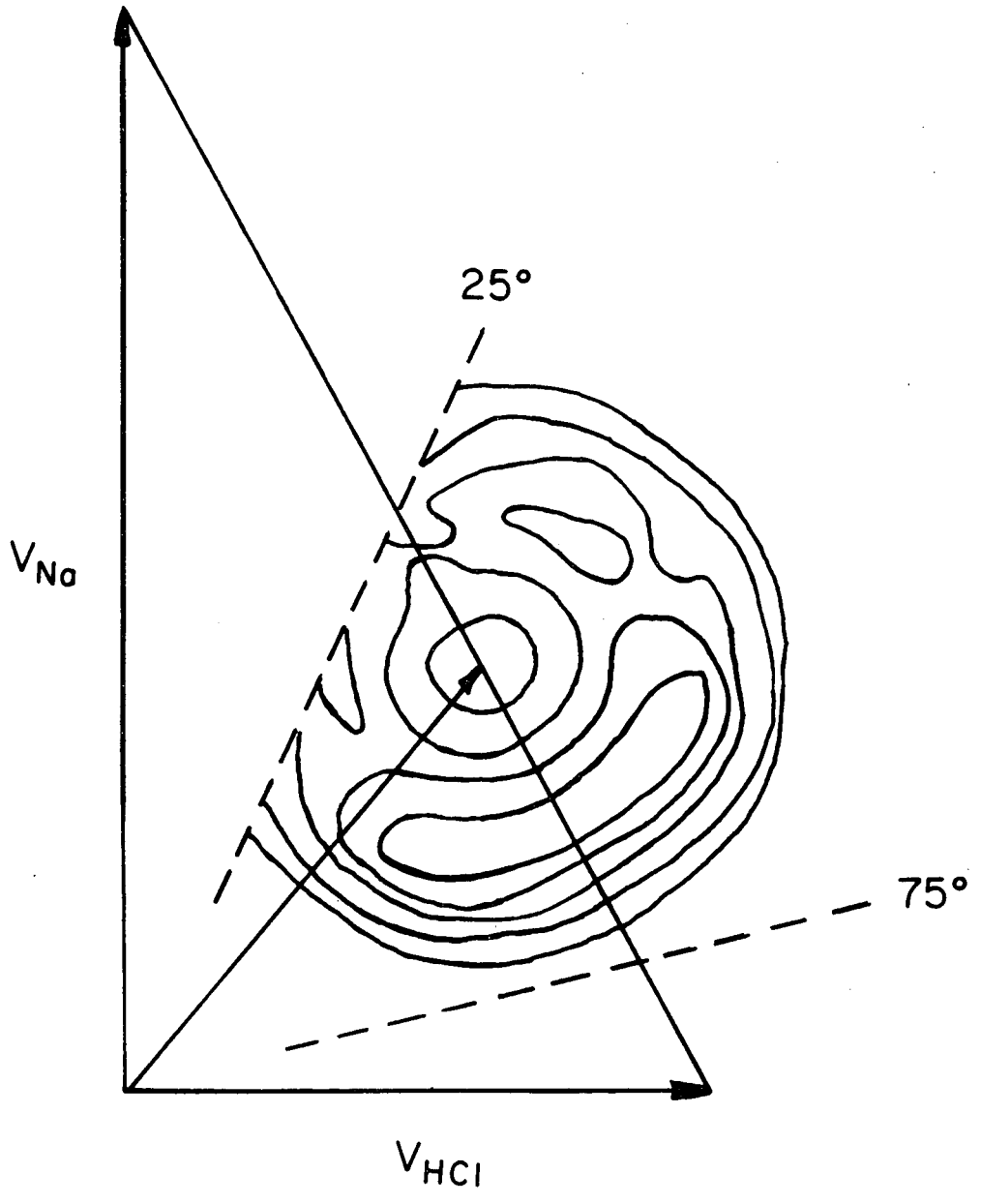

XBL 856-2876

Fig. 9

$$Na(3P) + HCl \longrightarrow NaCl + H \xrightarrow{e^-} \underline{Na}^+ + \cdots$$
$$E_{col} = 5.38\ kc/m$$

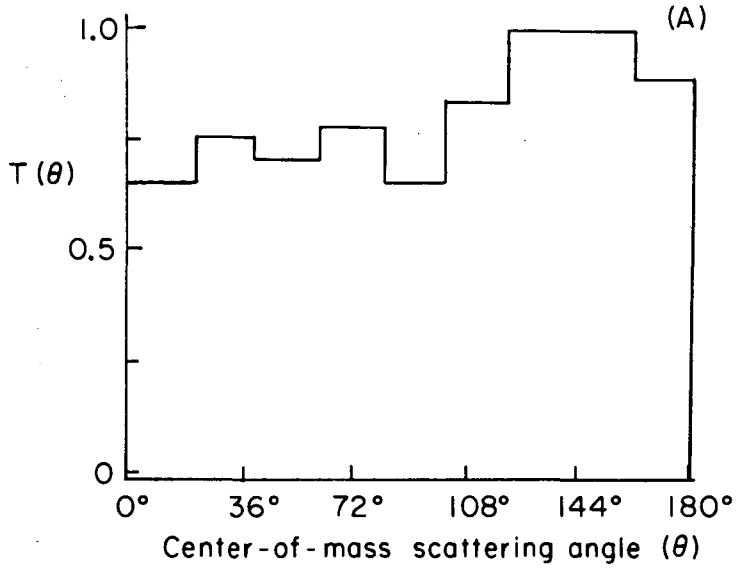

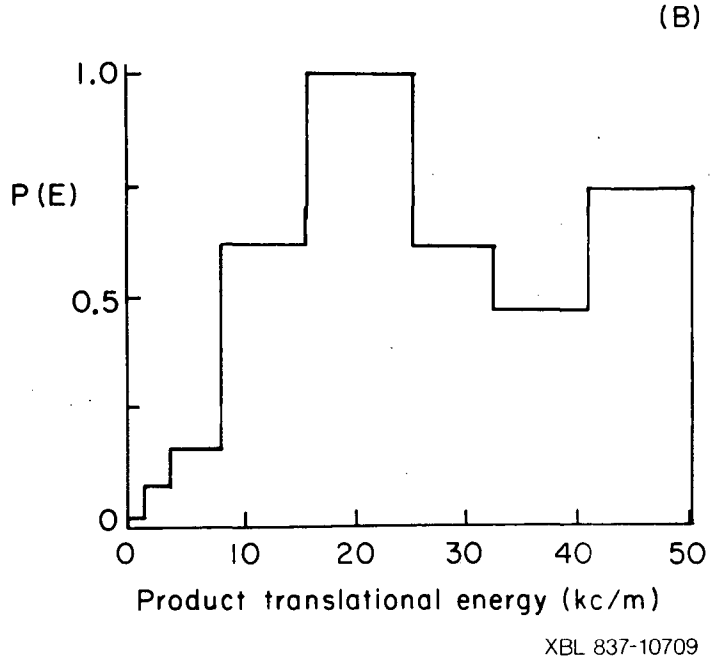

XBL 837-10709

Fig. 10

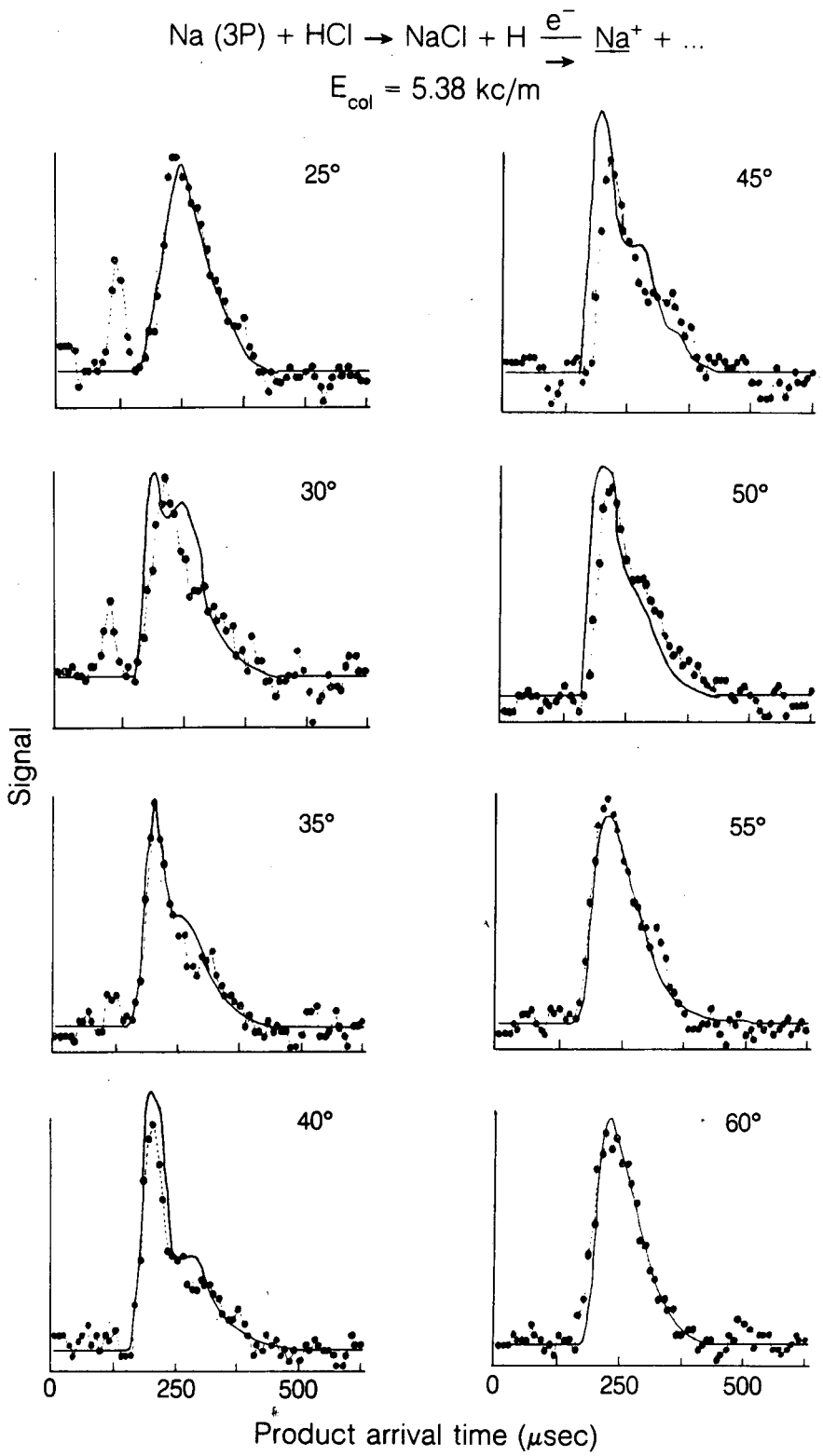

XBL 837-10707

Fig. 11

$$Na(3P) + HCl \longrightarrow NaCl + H \xrightarrow{e^-} Na^+ + \cdots$$
$$E_{col} = 5.35\,kc/m$$

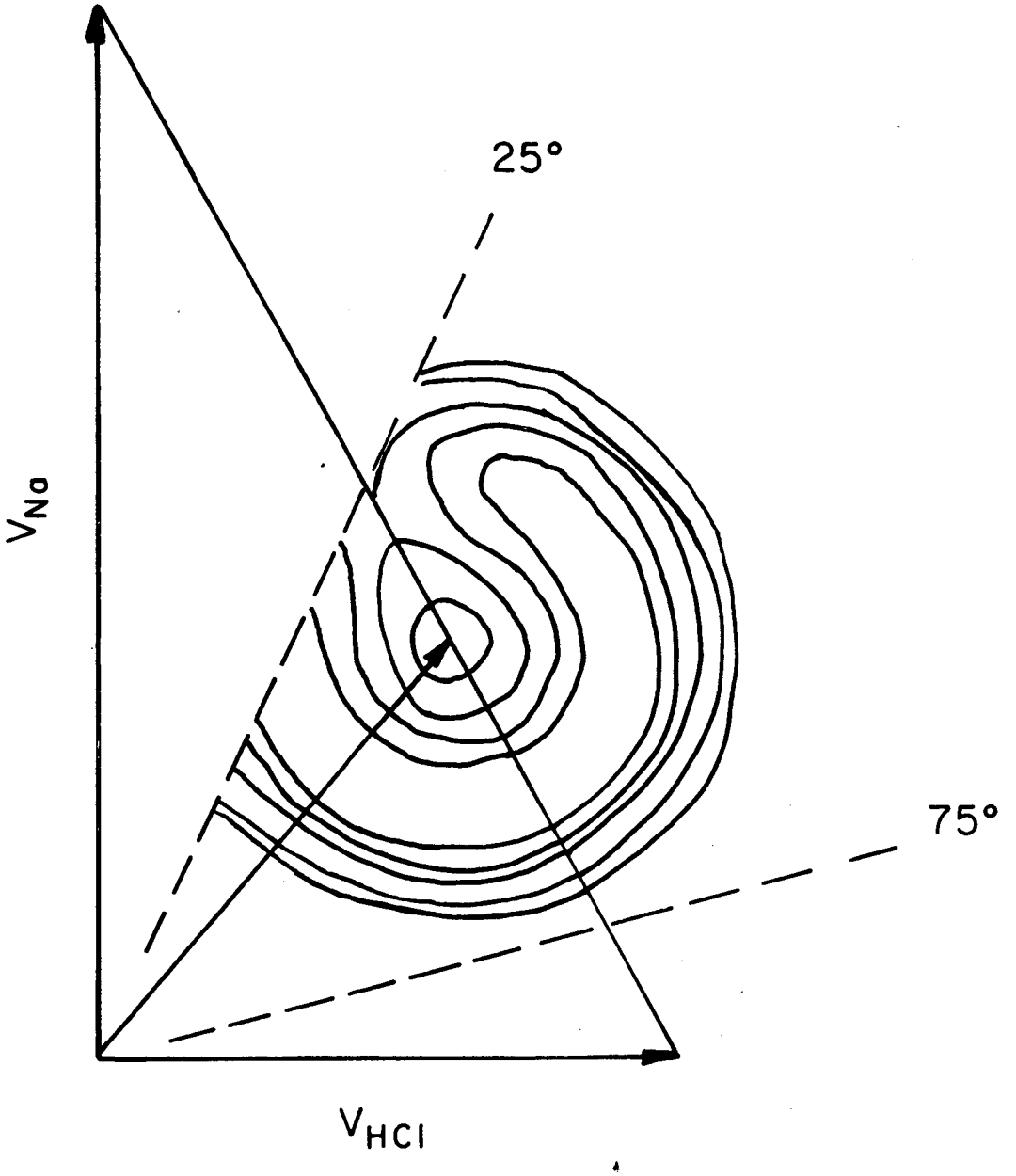

XBL 856-2875

Fig. 12

LAWRENCE BERKELEY LABORATORY
TECHNICAL INFORMATION DEPARTMENT
UNIVERSITY OF CALIFORNIA
BERKELEY, CALIFORNIA 94720